SELECTIVE IMAGE-SHARPNESS ENHANCEMENT BY COUPLED NONLINEAR REACTION-DIFFUSION TIME-EVOLUTION AND ITS PRACTICAL APPLICATION

Takahiro Saito, Jun Satsumabayashi, Kentarou Yashiro, Takashi Komatsu
Dept. of Electrical, Electronics and Information Engineering, Kanagawa University
3-27-1 Rokkakubashi, Yokohama, 221-8686, Japan
Tel: +81-45-481-5661; fax: +81-45-491-7915
e-mail:{saitot01,satsuj01,yashik01,komatt01}@kanagawa-u.ac.jp

ABSTRACT

This paper presents a method for selective sharpness enhancement that can sharpen only degraded edges blurred by several causes without increasing the visibility of nuisance factors such as random noise. The method is based on the coupled nonlinear reaction-diffusion time-evolution equipped with a second-order nonlinear smoothing term, a reaction term and an overshooting term. The quantitative performance evaluations demonstrate that the method sharpens blurred edges selectively much better than the existing sharpness enhancement methods such as the peaking method and the Volterra filter method. Moreover, this paper applies the method to the real problem of the breathing-distortion removal.

1. INTRODUCTION

As a classical method for image sharpness enhancement, the peaking technique [1] and its adaptive version [2] have been popular and used for practical applications such as the digital TV receiver's enhancement. And, recently another type of sharpness enhancement using nonlinear filters such as a Volterra filter has been proposed [3]. However, these existing methods have their own limitations; they cannot work well for blurred image heavily corrupted by random noise, and will produce the side effect that the noise visibility are augmented to some extent.

This paper shows that a sharpening method based on the coupled nonlinear reaction-diffusion time-evolution, a prototype of which was first proposed by M. Proesmans et al. [4], has an ideal capability to sharpen blurred edges without increasing the visibility of random noise. In this paper, along the analogous lines to the Proesmans's ones, we form a different scheme of the coupled nonlinear reaction-diffusion time-evolution based on the thin-plate-deflection second-order smoothness model in which the presented scheme differs from the Proesman's scheme. The presented nonlinear reaction-diffusion time-evolution is equipped with a second-order nonlinear smoothing term, a reaction term and an overshooting term. The coupled nonlinear reaction-diffusion method utilizes information about local image contents, to control the degree of the second-order smoothing and the magnitude of the overshoot to be added. The actual discrete expression for the time-evolution is defined as the iterative application of a local nonlinear operation, and the proposed time-evolution has a desirable property that computing a certain decision criterion will halt its iteration almost at the ideal moment when it achieves the best selective sharpness enhancement. The Proesmans's method does not include such a decision scheme to halt its iteration. We conduct quantitative performance evaluations using test images, and demonstrate that the presented method sharpens blurred edges selectively much better than the existing sharpness enhancement methods.

Moreover, to apply the method to the real problem of restoration of degraded image sequences, we introduce an adaptive control scheme into the presented method. We apply our reinforced method to the real problem to suppress the breathing distortion. The breathing distortion is caused by the phenomena of irregular temporal variations of focus, and we often experience in cinema.

2. NONLINEAR REACTION-DIFFUSION TIME-EVOLUTION FOR SHARPNESS ENHANCEMENT

2.1 Thin-Plate-Deflection Second-Order Smoothness Model

The idea of the reaction-diffusion is initiated by minimizing the functional:

$$E_g(f) = \iint \left[\left(u_x + v_y\right)^2 + \lambda \left\{ \left(u - f_x\right)^2 + \left(v - f_y\right)^2 \right\} + \frac{\sigma^2}{2} \cdot \left(f - g\right)^2 \right] dxdy \quad (1)$$

The functional is composed of the three terms. The second term penalizes approximation errors of two auxiliary functions u, v that approximate the first derivatives of the function f:

$$u \approx f_x \quad , \quad v \approx f_y \quad (2)$$

The approximations are introduced to lower the order of the Euler differential equations. The first term, the second-order smoothness term, detects f's meaningless variations by computing the deflection energy of a thin plate, whereas Proesmans employed the piecewise-rigid-plane second-order smoothness model [4]. The third term, the reaction term, penalizes f's deviations from the input g. Adding the reaction term with the parameter σ is suitable for image enhancement.

The Euler equations do not have clear physical meanings, because the coupled equations for the two auxiliary functions, u, v, have the cross derivative terms. Rewriting the equations to a simpler form that has the same solution of f under the condition of equation 2, we will obtain the resultant coupled equations:

$$\begin{aligned} &\sigma^2 \left(f - g\right) - 2\lambda \left(f_{xx} + f_{yy} \right) + 2\lambda \left(u_x + v_y \right) = 0 \\ &2\lambda \left(u - f_x \right) - 2 \left(u_{xx} + u_{yy} \right) = 0 \\ &2\lambda \left(v - f_y \right) - 2 \left(v_{xx} + v_{yy} \right) = 0 \end{aligned} \quad (3)$$

The above equations have clear physical meanings; all the three equations are categorized as a reaction-diffusion-type equation that has a diffusion term and a reaction term. The first equation has an additional term identical to the overshoot term of the peaking method, and it will produce overshoots in the vicinity of step edges while smoothing out meaningless random variations within a homogeneous region. Controlling their smoothing/overshooting behaviors, they would sharpen blurred edges without enhancing nuisance factors such as random noise. To control the degree of the

overshoots to be added, we introduce a shooting parameter s. Moreover, to avoid over-smoothing due to the linear diffusion, we introduce the concept of the nonlinear diffusion. Furthermore, introducing the artificially time-evolution variable τ, we obtain the partial differential equations for their time-evolution:

$$\begin{aligned}\frac{\partial f}{\partial \tau} &= div\left[c\left(\|\nabla f\|\right)\nabla f\right] - s\cdot\left(u_x + v_y\right) - \frac{\sigma^2}{2\lambda}\left(f-g\right)\\ \frac{\partial u}{\partial \tau} &= \frac{1}{\lambda}\left\{div\left[c\left(\|\nabla u\|\right)\nabla u\right] - \lambda\cdot\left(u - f_x\right)\right\}\\ \frac{\partial v}{\partial \tau} &= \frac{1}{\lambda}\left\{div\left[c\left(\|\nabla v\|\right)\nabla v\right] - \lambda\cdot\left(v - f_y\right)\right\}\end{aligned} \tag{4}$$

where the function c means the nonlinear diffusiveness function and in this paper is given by

$$c\left(\gamma\right) = 1\Big/\left\{1+\left(\gamma/K\right)^2\right\} \tag{5}$$

2.2 Piecewise-Rigid-Plane Second-Order Smoothness Model

M. Proesmans et al. previously presented another coupled nonlinear reaction-diffusion scheme [4]. Their method is different in that they adopt the piecewise-rigid-plane model, instead of the thin-plate-deflection model, as the second-order smoothness model. The piecewise-rigid-plane model measures the energy as follows:

$$\iint \left(f_{xx} + 2f_{xy} + f_{yy}\right)^2 dxdy \tag{6}$$

However, their derivation of the time-evolution equations from the energy functional lacks consistency; their derived time-evolution must be evaluated as a cross between the time-evolution based on the thin-plate-deflection model and that based on the piecewise-rigid-plane model.

Applying the analogous procedure to thin-plate-deflection model, we obtain another type of the time-evolution. Unfortunately, the derived time-evolution equations do not have so clear physical meanings as equation 4.

2.3 Discrete Form of the Time-Evolution

The actual discrete expression for equation 4 is defined as the iterative application of local nonlinear operations, as follows:

$$\begin{aligned}f_{i,j}^{\tau+1} &= f_{i,j}^{\tau} + \varepsilon\left[\sum_{d=N,S,E,W}\left\{C\left(\nabla_d f_{i,j}^{\tau}\right)\cdot\nabla_d f_{i,j}^{\tau}\right\}\right.\\ &\left. - \frac{s}{2}\left\{\left(u_{i+1,j}^{\tau+1} - u_{i-1,j}^{\tau+1}\right) + \left(v_{i,j+1}^{\tau+1} - v_{i,j-1}^{\tau+1}\right)\right\} - \frac{\sigma^2}{2\lambda}\left(f_{i,j}^{\tau} - g_{i,j}\right)\right]\\ &;\ \sum_{d=N,S,E,W}\left\{C\left(\nabla_d f_{i,j}\right)\cdot\nabla_d f_{i,j}\right\} = C\left(\nabla_N f_{i,j}\right)\cdot\nabla_N f_{i,j} +\\ &\quad C\left(\nabla_S f_{i,j}\right)\cdot\nabla_S f_{i,j} + C\left(\nabla_E f_{i,j}\right)\cdot\nabla_E f_{i,j} + C\left(\nabla_W f_{i,j}\right)\cdot\nabla_W f_{i,j}\\ &\quad ,\ \nabla_N f_{i,j} = f_{i,j-1} - f_{i,j}\ ,\ \nabla_S f_{i,j} = f_{i,j+1} - f_{i,j}\\ &\quad ,\ \nabla_E f_{i,j} = f_{i+1,j} - f_{i,j}\ ,\ \nabla_W f_{i,j} = f_{i-1,j} - f_{i,j}\\ u_{i,j}^{\tau+1} &= u_{i,j}^{\tau} + \frac{\varepsilon}{\lambda}\left[\sum_{d=N,S,W,E}\left\{C\left(\nabla_d u_{i,j}^{\tau}\right)\cdot\nabla_d u_{i,j}^{\tau}\right\}\right.\\ &\quad \left. - \lambda\left\{u_{i,j}^{\tau} - \frac{1}{2}\cdot\left(f_{i+1,j}^{\tau} - f_{i-1,j}^{\tau}\right)\right\}\right]\\ v_{i,j}^{\tau+1} &= v_{i,j}^{\tau} + \frac{\varepsilon}{\lambda}\left[\sum_{d=N,S,W,E}\left\{C\left(\nabla_d v_{i,j}^{\tau}\right)\cdot\nabla_d v_{i,j}^{\tau}\right\}\right.\\ &\quad \left. - \lambda\left\{v_{i,j}^{\tau} - \frac{1}{2}\cdot\left(f_{i,j+1}^{\tau} - f_{i,j-1}^{\tau}\right)\right\}\right]\end{aligned} \tag{7}$$

The initial setting is given by

$$f_{i,j}^{0} = g_{i,j}\ ;\ u_{i,j}^{0} = \left(g_{i+1,j} - g_{i-1,j}\right)/2\ ;\ v_{i,j}^{0} = \left(g_{i,j+1} - g_{i,j-1}\right)/2 \tag{8}$$

In this paper, as a decision scheme to halt its iteration, we employ the following scheme:

$$\begin{aligned}&if\ \left|\delta^{\tau-1,\tau} - \delta^{\tau,\tau+1}\right| \le \delta_T\ ,\quad then\ stop\ the\ iteration.\\ &;\ \delta^{\tau,\tau+1} \triangleq \delta_f^{\tau,\tau+1}\Big/\delta_{uv}^{\tau+1}\quad ,\quad \delta_f^{\tau,\tau+1} \triangleq \sum_{i,j}\left|f_{i,j}^{\tau+1} - f_{i,j}^{\tau}\right|\Big/\sum_{i,j}1\ ,\\ &\delta_{uv}^{\tau+1} \triangleq \sum_{i,j}\{|u_{i,j}^{\tau+1}| + |v_{i,j}^{\tau+1}|\}\Big/(2\cdot\sum_{i,j}1)\end{aligned} \tag{9}$$

Our proposed time-evolution of equation 7 has a desirable property that the above decision scheme will halt its iteration almost at the ideal moment when it achieves the best selective sharpness enhancement. In most cases, the time-evolution of equation 7 will be stopped within *100* iterations, and will take less than *15* seconds per image of *512* by *512* pixels on a PC with a single *1 GHz* Pentium IV processor. The Proesmans's method does not include such a decision scheme to halt its iteration, and their time-evolution sometimes cannot be stopped.

2.4 Performance Evaluation Using Test Images

We evaluate performance of our method using artificially blurred test images. First we blur an original sharp image $h(x,y,t)$ with the Gaussian filter having the impulse response $G(x,y\,;\,\zeta)$,

$$G(x,y;\zeta) = \frac{1}{2\pi\zeta^2}\cdot\exp\left(-\frac{(x^2+y^2)}{2\zeta^2}\right) \tag{10}$$

and then add random Gaussian noise $n(x,y,t)$ to the blurred image $G*h(x,y,t)$; thus we generate an artificially blurred test image $g(x,y,t)$. The image $f(x,y,t)$ denotes the sharpness-enhanced image reproduced from the blurred test image $g(x,y,t)$.

For the performance evaluation we define the qualitative measures as follows:

(1) *SNR of the sharpened image*: *SNR* is computed between the original sharp image h and the sharpened image f. The decision scheme of equation 9 can halt the iteration of our proposed time-evolution of equation 7 almost at the moment when it attains its maximum *SNR*.

(2) *Blur-Removal Ratio Br & Noise-Removal Ratio Nr*: The vectors, **b**, **n**, **s**, denote Gaussian-blurs artificially added to the original image h, random Gaussian noise components added to the Gaussian blurred image $G*h$, and deviations of the artificially blurred test image g from the sharpened image f, i.e. $g-f$, respectively. We define the vectors by putting their respective values at all the pixels in a column. Then, we define the blur-removal ratio Br and the noise-removal ratio Nr as follows:

$$Br = \left(\mathbf{b},\mathbf{s}\right)\Big/\|\mathbf{b}\|^2\quad ,\quad Nr = \left(\mathbf{n},\mathbf{s}\right)\Big/\|\mathbf{n}\|^2 \tag{11}$$

The positive value of Br/Nr means that the blur/noise removal is successfully achieved. If blur/noise is perfectly removed, then the value of Br/Nr will be *1.0*; but the reverse is not necessarily true. On the contrary, the negative value means that the blur/noise is augmented far from being removed.

(3) *Average Contrast C* [5]: For each pixel, first we compute the contrast $C_{(f)}(x,y,t)$ for the sharpness-enhanced image $f(x,y,t)$ as follows:

$$\begin{aligned}C_{(f)}(x,y,t) &= \frac{\left|f(x,y,t) - E_{(f)}(x,y,t)\right|}{f(x,y,t) + E_{(f)}(x,y,t)}\\ &,\ E_{(f)}(x,y,t) = \frac{\sum_{(k,l)\in N(x,y,t)}\Delta_{(f)}(k,l,t)\cdot f(k,l,t)}{\sum_{(k,l)\in N(x,y,t)}\Delta_{(f)}(k,l,t)}\end{aligned} \tag{12}$$

where $\Delta_{(f)}(x,y,t)$ is the edge value computed using Sobel row and column operators and $E_{(f)}(x,y,t)$ is the mean edge value computed in a

3 by *3* neighborhood $N(x,y,t)$ of the pixel located at pixel coordinates (x,y,t). The value of the contrast C is highest at intensity discontinuities that occur along edges. Then we average the contrast $C_{(f)}(x,y,t)$ over the image f, thus estimating the average contrast $C_{(f)}(t)$:

$$C_{(f)}(t) = \mathbf{E}_{(x,y)}\left[C_{(f)}(x,y,t)\right] \tag{13}$$

First we set the blurring parameter ζ in equation 10 as *1.0*, and set the sharpness enhancement parameters λ, σ, K as *1.0*, *1.0*, *5.0*, respectively. Changing the shooting parameter s, we apply the presented sharpness improvement method to the blurred test image. Figure 1 shows the values of $C_{(f)}$, Br, and Nr versus the shooting parameter s. Figure 1 shows the results of our method based on the thin-plate-deflection model of equation 7. Our method achieves the satisfactory selective sharpness enhancement; only blurred edges are sharpened without amplification of random noise.

Next, we set the sharpness enhancement parameters λ, s, σ, K as *1.0*, *0.5*, *1.0*, *5.0*, respectively. Changing the blurring parameter ζ in equation 10, we apply the presented method to the artificially blurred test image g. Figure 2 shows the average contrast $C_{(f)}$ of the sharpened image f versus the blurring parameter ζ, and also shows the average contrast $C_{(g)}$ of the artificially blurred test image g and the average contrast $C_{(h)}$ of the original sharp image h. Our method based on the thin-plate-deflection model behaves almost ideally; if the Gaussian blurring parameter ζ is less that *1.0*, it will recover image sharpness nearly to the equal level. The other methods do not have such a property.

Figure 3 shows the blurred test image and the image sharpened by the presented method and the images sharpened by the adaptive peaking method [2] and the adaptive Volterra filter method [3]. From figure 3, we find that the presented method successfully achieves selective sharpness enhancement, and gives the subjectively best quality sharpened image.

3. SUPPRESSION OF BREATHING DISTORTIONS

We apply our coupled reaction-diffusion based method of equation 7 to the real problem to suppress the breathing distortions. The breathing distortion is caused by the phenomena of irregular temporal variations of focus. We often experience the breathing distortion in cinema. The image sequence containing the breathing distortion looks like a motion picture irregularly moving in and out of focus. Sometimes, images are randomly blurred due to irregular defocus. Figure 4 shows the average contrast $C_{(f)}$ of the sharpened image f versus the average contrast $C_{(g)}$ of the blurred image g for each input blurred image frame g of the real old film sequence containing the breathing distortions. As shown in figure 4, if the shooting parameter s is fixed, the average contrast $C_{(f)}$ of the sharpened image sequence will fluctuate frame by frame and the breathing distortions cannot be suppressed.

If an input image frame is heavily blurred, to sharpen it to the prescribed level of the average contrast it will be desirable that the shooting parameter s should be made large at the cost of some augmentation of random noise visibility. To improve the efficiency of suppression of the breathing distortions, we reinforce the presented method with the adaptive scheme that controls the shooting parameter s as a decreasing function of the average contrast $C_{(g)}$ of each input blurred image frame g. We introduce an adaptive scheme of changing the shooting parameter s as a stepwise function of the average contrast $C_{(g)}$ of the input frame g. The stepwise adaptive control is designed as follows: examining the characteristics as shown in figure 4 for an input image sequence, first we determine the target level of the average contrast $C_{(f)}$ of the sharpened image frame f, and as the shooting parameter s for every input frame we select the smallest value that can attain the target average contrast. The resultant adaptive control scheme is expressed as the swithchover-type logic as follows:

$$\textit{if} \quad C_i \le C_{(g)} < C_{i+1}\,, \quad \textit{then} \quad s = s_i\,. \tag{14}$$

We apply our adaptive method to real old film sequences containing the breathing distortions. Figure 5 shows the average contrast $C_{(f)}$ of each image frame f sharpened by our adaptive scheme, along with the average contrast $C_{(g)}$ of the input frame g. The results of experimental simulations demonstrate that our adaptive method suppresses the breathing distortions very efficiently and produces the uniformly focused image sequence.

4. CONCLUSIONS

The quantitative performance demonstrate that our method sharpens blurred edges selectively much better than the existing methods. Moreover, introducing the adaptive scheme, we reinforce it and apply it to the suppression of the breathing distortions.

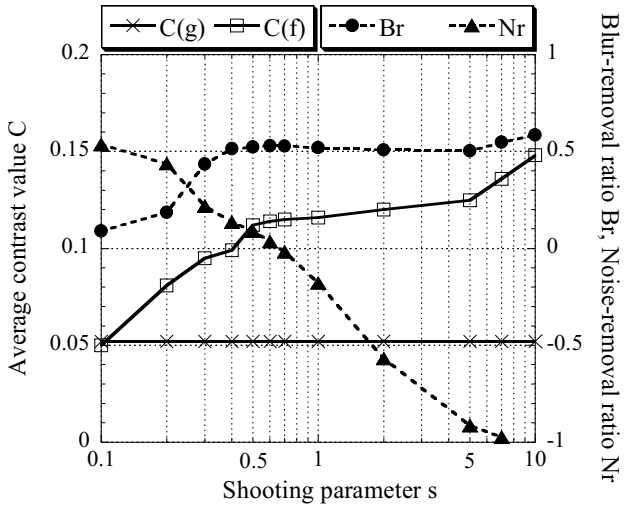

Figure 1. Average contrast $C_{(f)}$ of the sharpened image f and the blur-removal ratio Br and the noise-removal ratio Nr versus the shooting parameter s under the blurring parameter (ζ) = *1.0* and the parameter setting of (λ, σ, K) = (*1.0*, *1.0*, *5.0*).

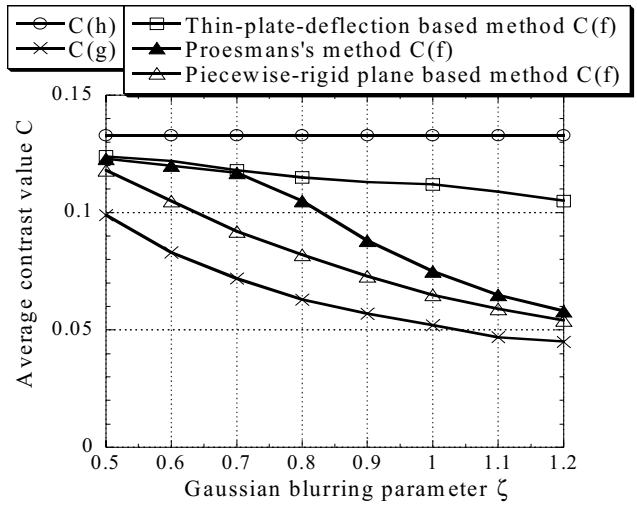

Figure 2. Average contrast $C_{(f)}$ of the sharpened image f versus the blurring parameter ζ under the parameter setting of (λ, s, σ, K) = (*1.0*, *0.5*, *1.0*, *5.0*).

(a) Blurred test image of the blurring parameter (ζ) = *1.0*
[*SNR = 20.175*[*dB*], $C_{(g)} = 0.052$]

(b) Sharpened image by the thin-plate-deflection based method of the parameter setting of (λ, *s*, σ, *K*) = (*1.0*, *0.5*, *1.0*, *5.0*)
[*SNR = 22.882*[*dB*], $C_{(f)} = 0.112$, *Br = 0.513*, *Nr = 0.136*]

(c) Sharpened image by the adaptive peaking method [2]
[*SNR = 21.416*[*dB*], $C_{(f)} = 0.097$, *Br = 0.310*, *Nr = -1.065*]

(d) Sharpened image by the adaptive Volterra filter method [3]
[*SNR = 21.320*[*dB*], $C_{(f)} = 0.070$, *Br = 0.258*, *Nr = -0.724*]

Figure 3. Blurred test image and sharpened images given by the several selective sharpness enhancement methods.

REFERENCES

[1]A. Rosenfeld and A.C. Kak, "Digital picture processing", Ch.6.4.2., Academic Press, Inc., New York, 1982.

[2]E.G.T. Jaspers and P.H.N. de With, "A generic 2D sharpness enhancement algorithm for luminance signals", *Proc. IEE Int'l. Conf. IPA97*, pp.263-273, 1997.

[3]S. Thurnhofer and S.K. Mitra., "A general framework for quadratic Volterra filters for edge enhancement", *IEEE Trans. Image Process.*, **5**, pp.950-963, 1996.

[4]M. Proesmans, E.J. Pauwels, L.J. Van Gool, "Coupled geometry driven diffusion equations for low-level vision", Geometry-Driven Diffusion in Computer Vision, B.M. ter Haar Romeny (Ed.), pp.191-228, Kluwer, Dordrecht, 1994.

[5]A. Beghdadi and A.L.Negrate, "Contrast enhancement technique based on local detection of edges", *Computer Vision, Graphics and Image Understanding*, **46**, pp.162-174, 1989.

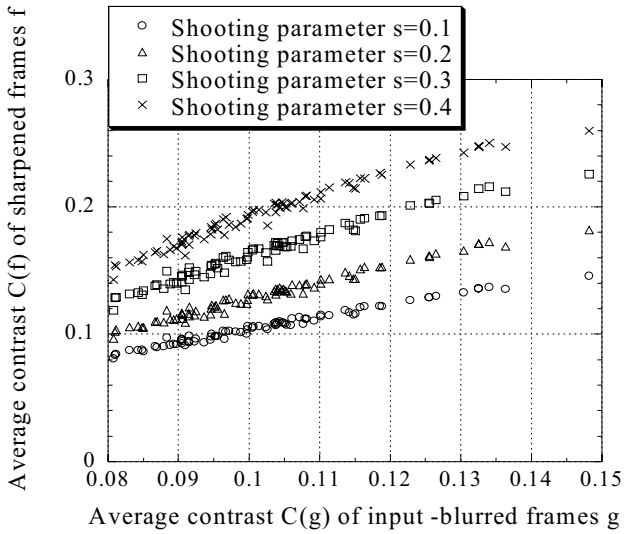

Figure 4. Average contrast $C_{(f)}$ of the sharpened image *f* versus the average contrast $C_{(g)}$ of the blurred input image *g* for each input image frame of the real old film sequence containing the breathing distortions.

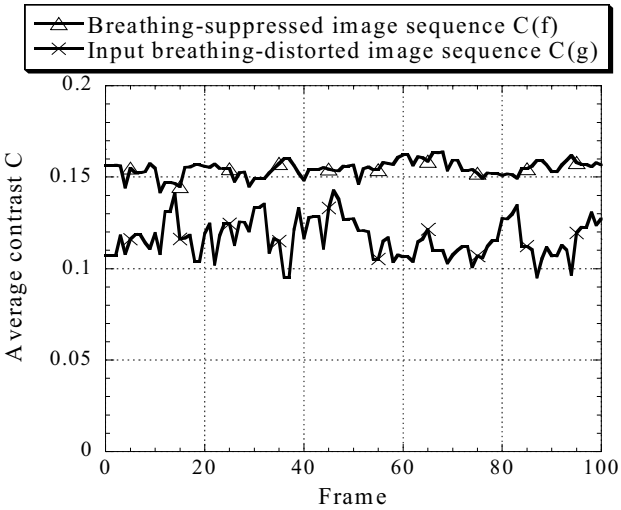

Figure 5. Average contrast $C_{(f)}$ of each image frame *f* sharpened by our adaptive scheme for the real old film sequence containing the breathing distortions.